coatings

MDPI

Article

Consolidation of Fragile Oracle Bones Using Nano Calcium Sulfate Hemihydrate as a Protectant

Yan Liu [1,2,3], Ruicong Lu [1,2,3], Lu He [1,2,3], Ximan Wang [1,2,3], Lu Wang [1,2,3], Xinyan Lv [1,2,3], Kun Zhang [1,2,3] and Fuwei Yang [1,2,3,*]

[1] China-Central Asia "the Belt and Road" Joint Laboratory on Human and Environment Research, Northwest University, Xi'an 710127, China; liuyan@nwu.edu.cn (Y.L.); 18066717745@163.com (R.L.); hl272103599@gmail.com (L.H.); wangximan996@163.com (X.W.); lwang810@foxmail.com (L.W.); 202120969@stumail.nwu.edu.cn (X.L.); 20199013@nwu.edu.cn (K.Z.)
[2] Key Laboratory of Cultural Heritage Research and Conservation, Northwest University, Xi'an 710127, China
[3] School of Culture Heritage, Northwest University, Xi'an, 710127, China
* Correspondence: yangfuwei@nwu.edu.cn

Abstract: Herein, a nano calcium sulfate hemihydrate suspension in an alcohol solvent was prepared and explored as a novel protectant for fragile oracle bones. The consolidation method involved first introducing the suspension and then adding water into the bones. Through this method, cohesive calcium sulfate dihydrate formed in the bones and can act as a reinforcing material. The protective effect was studied by scanning electron microscopy (SEM), energy dispersive X-ray spectroscopy (EDX), Fourier transform infrared spectroscopy (FTIR), X-ray diffractometry (XRD), hardness, porosity, and color difference determination. The results showed that such consolidation increased the strength of the bone samples significantly, and only slightly changed the appearance and porosity of the bone samples, indicating a good prospect for applying nano calcium sulfate hemihydrate in the conservation of indoor fragile bone relics.

Keywords: consolidating agent; bone relics; nano suspension; calcium sulfate hemihydrate

check for updates

Citation: Liu, Y.; Lu, R.; He, L.; Wang, X.; Wang, L.; Lv, X.; Zhang, K.; Yang, F. Consolidation of Fragile Oracle Bones Using Nano Calcium Sulfate Hemihydrate as a Protectant. *Coatings* **2022**, *12*, 860. https://doi.org/10.3390/coatings12060860

Academic Editor: Gabriela Graziani

Received: 12 May 2022
Accepted: 16 June 2022
Published: 18 June 2022

Publisher's Note: MDPI stays neutral with regard to jurisdictional claims in published maps and institutional affiliations.

Copyright: © 2022 by the authors. Licensee MDPI, Basel, Switzerland. This article is an open access article distributed under the terms and conditions of the Creative Commons Attribution (CC BY) license (https://creativecommons.org/licenses/by/4.0/).

1. Introduction

Oracle bones are animal bones that were used in the divination events of ancient China [1]. This type of bone divination dated back to as early as the late-Neolithic Age and flourished in the Shang Dynasty [2,3]. Inscriptions on the bones are believed to be the earliest Chinese characters and thus oracle bones are important for study on the early civilization of ancient China [4]. Unfortunately, the excavated oracle bones are often fragile as a result of the special processing procedure in divination and the long burial time of the bones [5]. Calcination is necessary in the preparation of oracle bones, the process in which the organic materials including collagen and fat in the bones are burnt out [6]. Additionally, some inorganic minerals such as calcium carbonate and carboxyapatite are partly dissolved during the long burial time [7]. The loss of the total organic matter and part of the inorganic minerals as described above leads to the decreased bulk density and mechanic strength of the oracle bones. Consolidation treatment on the bones is thus necessary for their preservation.

For a long time, organic materials such as paraffine, acrylic, and silicone resins have been the most widely used consolidating agents. They can work as glues and confer strength to weak bones once again. However, these organic consolidants are not sufficient in terms of weatherability and are apt to aging under photo damage, atmospheric oxidation, and microbial erosion [8]. After aging, their protective function decreases sharply, and negative consequences such as yellowing, embrittlement, and shrinkage occur, leading to the "preservation damage" of bone objects [9].

Due to their good weatherability, inorganic protective materials have been tested as alternatives. Calcium hydroxide was studied as a reinforcement material in archeological bones by Natali I. et al. [10]. After its introduction into the bone sample, it can react with carbon dioxide in the air and produce an adhesive aragonite. North A. et al. [11] studied the effect of ammonium hydrogen phosphate, which can react with calcite in the bone matrix and produce hydroxyapatite, thereby increasing the cohesiveness of the friable bones. Hydroxyapatite colloid was used directly as a consolidating agent of archeological ivories by Gong W. et al. [12] as it can be deposited on the surface of the ivories and form a strengthening layer. Recently, Liu Y. et al. [13] successively introduced a nano calcium hydroxide suspension and a solution of ammonium sulfate into bones, which could form calcium sulfate dihydrate and consolidate bone relics. Calcium sulfate dihydrate, also known as gypsum, has long been widely used in the repair of museum collections such as in pottery, porcelain, bones, and even metal wares [14–16]. It is stable enough and can hardly be aged in the museum environment. Calcium sulfate dihydrate can even be selectively cleared away by the scavenging agent of barium carbonate [17], making it a potential reversible protective material. However, the strategy of using calcium hydroxide and ammonium sulfate as the precursors of calcium sulfate dihydrate in a previous study [13] is challenging in practical applications. First, the distribution of calcium hydroxide and ammonium sulfate in the bone substrate is not uniform, which is also the case of the resulting gypsum product and its consolidation effect. Second, the irritant ammonia gas will be generated during the treatment process, which is an undesirable by-product during the reaction between calcium hydroxide and ammonium sulfate.

Hence, in this paper, a suspension of nano calcium sulfate hemihydrate in an alcohol solvent was prepared and explored as a novel consolidating agent for oracle bones under an indoor environment. The suspension liquid was introduced into the bone samples by surface permeability and then hydrated into an adhesive calcium sulfate dihydrate, which is illustrated in Figure 1. Due to the formation of the calcium sulfate dihydrate, the pores and cracks in the weathering bone samples were filled and the integrity of the samples was reestablished. The consolidation effect was evaluated by scanning electron microscopy (SEM), energy-dispersive X-ray spectroscopy (EDX), X-ray diffractometry (XRD), hardness, porosity, and color difference determination.

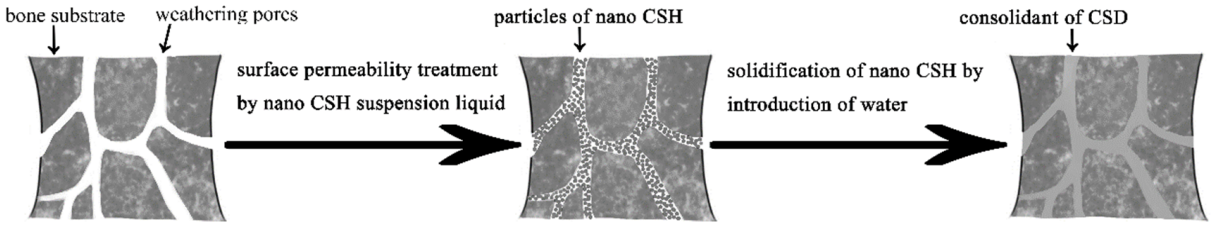

Figure 1. The schematic representation of the consolidation mechanism.

2. Experimental

Analytical grade reagents of calcium chloride ($CaCl_2$), 2-propanol (C_3H_8O), and sulfuric acid (H_2SO_4) were purchased from Sinopharm Group Co. Ltd., Shanghai, China. The suspension of nano calcium sulfate hemihydrate (CSH) in an alcohol solvent was prepared as follows. Anhydrous calcium chloride and sulfuric acid (90%) were first dissolved in ethylene glycol to yield a solution at concentration of 0.5 mol/L, respectively. Then, these two solutions were mixed equally to prepare the precipitate of CSH. After centrifugation and washing, the precipitate was re-dispersed in 2-propanol to produce a suspension with a concentration of 10 g/L.

The artificial oracle bones were prepared according to one of our previous studies [13]. The cow bones (1.0 cm × 1.0 cm × 2.0 cm) were calcined at 650 °C, soaked in a 4.5% solution of hydrochloric acid, washed with pure water, and finally dried naturally. Due to the loss of all of the organic collagens and part of the inorganic minerals, the artificially

weathered bones are extremely similar to the archeological bones in terms of their chemical composition and physical properties.

The consolidation process of the bone samples is as follows. First, the suspension liquid of nano CSH was introduced into the bone samples by surface permeability. Then, the nano CSH was hydrated into calcium sulfate dihydrate (CSD) under a constant humidity of 85%. With the formation of CSD, additional cohesion was obtained and the weak bones were strengthened. The porosity and bulk density of the samples were determined by Picnometer Accupyc II 1240-Micromeritics (Centro di Geotecnologie, University of Siena, Siena, Italy). The mechanical strength of the samples was evaluated by a micro-hardness tester (HD-3000L, Shenzhen Wallok Testing Equipment Technology Co., Ltd., Shenzhen, China). The appearance change (ΔE) of the samples was evaluated by a reflectance spectrophotometer (WSC-S, D65 illuminant, 8°/d optical geometry, XiangYi Instrument (Xiangtan) Co., Ltd., Xiangtan City, China). The addition amount of nano CSH was 5–10% of the mass of the bone samples.

Scanning electron microscopy (SEM, FEI SIRION-100, 5.0 kV of accelerating voltage and 8.0 mm of working distance, Hillsboro, OR, USA) with energy-dispersive X-ray spectroscopy (EDX), Fourier transform infrared spectroscopy (FTIR, Nicolet 560, 4000–450 cm^{-1} range), and X-ray diffractometry (XRD, AXS D8 ADVANCE, Cu Ka radiation, scan range 2θ = 10–80°, Bruker, Billerica, MA, USA) were used to analyze the structure and composition of the samples. These analyses were performed on samples treated with 7% nano CSH.

The kinetic stability of the suspension liquid of nano CSH was evaluated by the absorbance measure at 300 nm using an ultraviolet/visible spectrophotometer (Varian Cary 100, SpectraLab Scientific Inc., Markham, ON, Canada).

3. Results and Discussion

The prepared calcium sulfate hemihydrate (CSH) suspension in 2-propanol is shown in Figure 2, which has a kind of milky liquid appearance. The micro-morphology and elemental composition of the CSH particles in the suspension are shown in Figure 3. The particles were stumpy and the size distribution roughly fits a Gaussian distribution with a range of 80–600 nm and the center distribution was about 200 nm (Figure 3b inset). This size scale is smaller compared to some of the previous studies, in which the particle sizes were usually bigger than 400 nm [18,19], and this smaller particle size is beneficial for good permeability. The particles are composed of O, S, and Ca elements from the EDX results. The phase composition of these particles was further confirmed by the XRD results in Figure 4. In the past, α-CSH and β-CSH were believed to be hardly distinguished by XRD spectra. However, according to recently published research [20], the peak position around 2θ = 30° shows a slight difference for the two kinds of CSH phases: the one for α-CSH is located at around 2θ = 29.80°, while this peak position for β-CSH is around 2θ = 29.70°. Therefore, the nano CSH particles presented here can be identified as the α type of the CSH from the aforementioned peak position located at 2θ = 29.81°. Additionally, the morphology of the CSH particles was also highly similar to that of the α-CSH observed by other researchers [21].

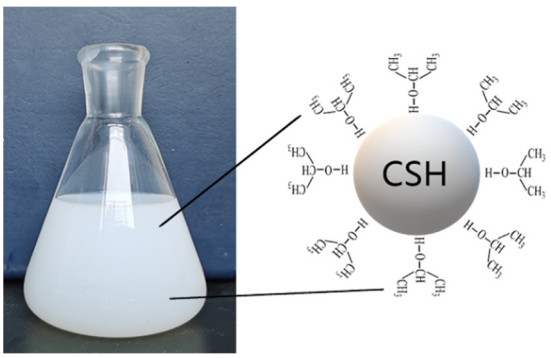

Figure 2. The CSH suspension in 2-propanol.

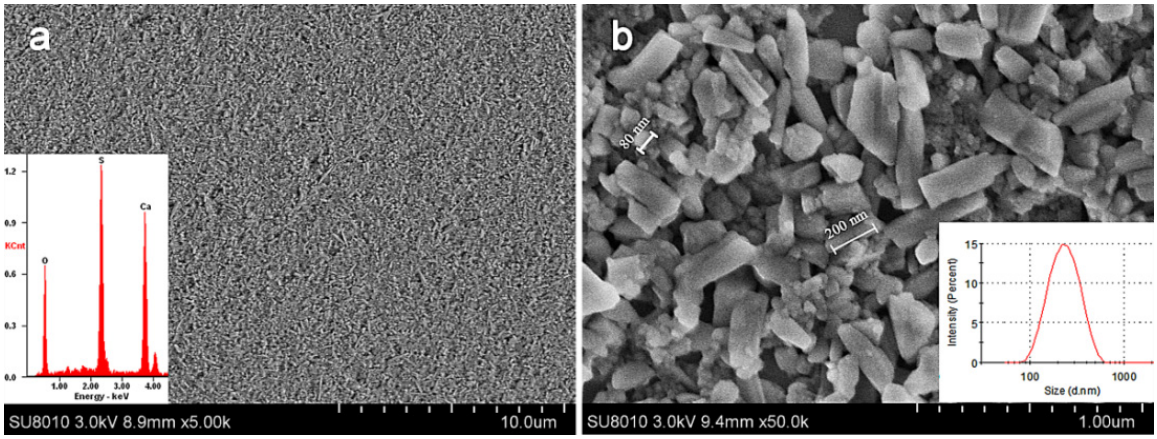

Figure 3. The SEM images of the CSH particles in the suspension liquid. (**a**) ×5000, (**b**) ×50,000.

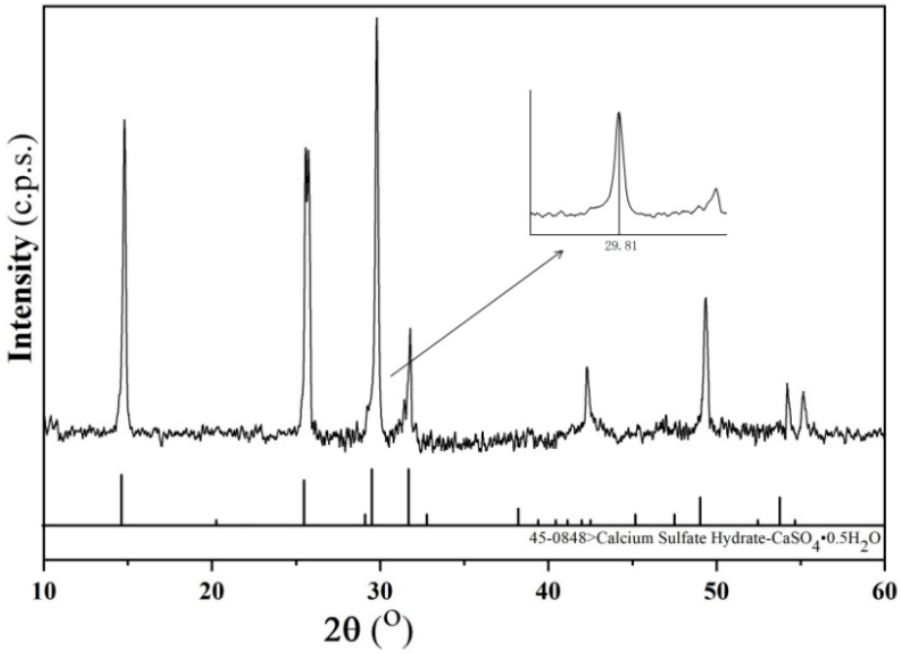

Figure 4. The XRD results of the CSH particles.

The suspension stability of CSH in 2-propanol was evaluated by absorbance measurements and the results are shown in Table 1. The absorbance was nearly constant during the test time, indicating a high kinetic stability of the suspension, which is due to both the small size of the CSH particles and the high steric hindrance of 2-propanol. As shown in Figure 2, 2-propanol absorbs on the surface of the CSH particles and forms an organic shield, which prevents agglomeration of the particles and setting of the suspension liquid [22]. This high stability of the nano materials in organic solvents has also been confirmed by previous studies, which is much better than in water (absorbance decreased to about 25% after 6 h) [23,24]. Stability is critical for a CSH suspension in practical applications, since it contributes to a deeper penetration of CSH into the open pores and cracks of the weathering bones to be consolidated.

Table 1. The kinetic stability of the CSH suspension.

Time (Hour)	0	1	2	3	4	5	6
Absorbance (%)	100	98	96.5	95	94.5	94.2	92

The morphology changes of the bone samples before and after treatment by the CSH suspension liquid are presented in Figure 5. As displayed in Figure 5a, the artificial oracle bone was coarse, porous, and loose due to the loss of the organic and inorganic components during the burning and subsequent burial process [25]. The suspension liquid of the nano CSH in 2-propanol was introduced into the bone sample by surface impregnation. After treatment, the open pores and fissures of the sample were patched up and the micro-structure seemed to be denser and flatter, as shown in Figure 5b. However, the particles of CSH were completely independent of each other at this time and can only serve as fillers. After the successive hydration treatment, further changes can be observed in Figure 5c,d. The separate CSH particles integrated together and a new board-like continuous structure was formed. This is mainly due to the dissolution–precipitation mechanism for the hydration of CSH [26]. As the hydration proceeds, the CSH is dissolved and then reorganizes to crystalline CSD [27]. In general, the typical morphology of the CSD is needle-like. However, its growth and morphology can be affected by the underlying matrix [10]. Here, we obtained a CSD with a board-like continuous structure, which may be related to the hydroxyapatite component of the bone samples.

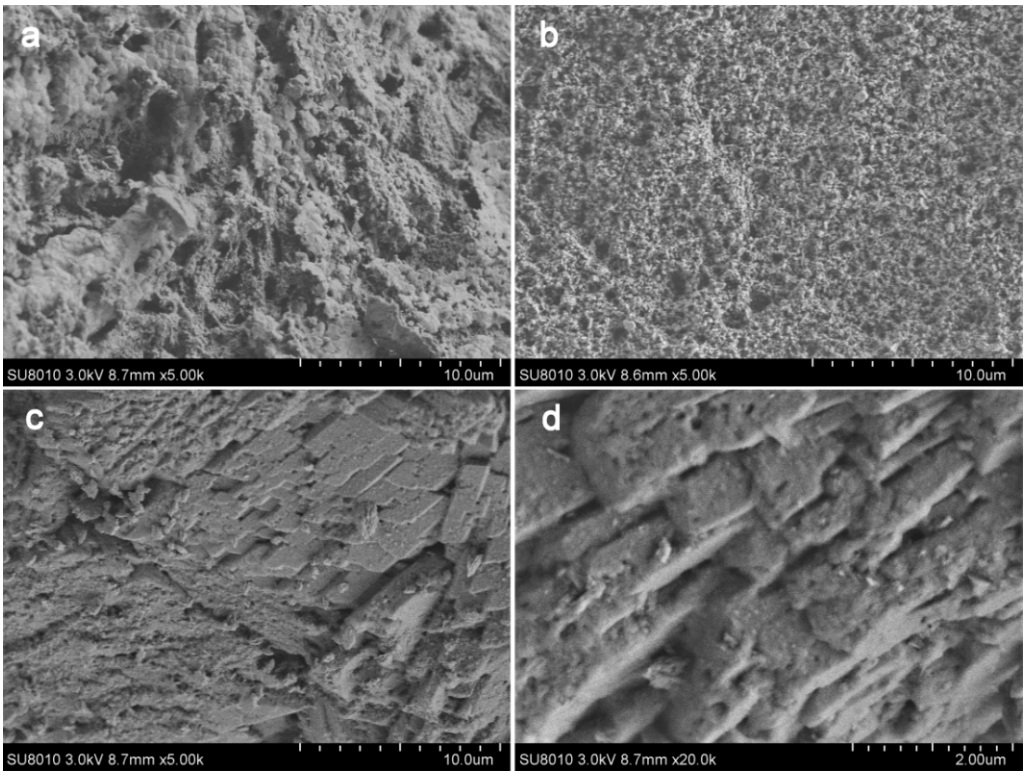

Figure 5. The micro-structure evolution of the bone samples. (**a**) Untreated, (**b**) treated by CSH, (**c**,**d**) treated by both CSH and water.

To investigate the possible mechanism of the morphology above, the composition of the bone samples was monitored during the consolidating process by FTIR and XRD analysis. The PO_4^{3-} bands (1090, 1018, 961, 606, 561 cm^{-1}) and the –OH bands (3555, 1633 cm^{-1}) in a in Figure 6 were from the bone sample, which was mainly composed of hydroxyapatite [28]. After the introduction of nano CSH particles in the bone sample, the SO_4^{2-} bands (1141, 666 and 601 cm^{-1}) and typical O–H band at 3612 cm^{-1} appeared in b in Figure 6 and were assigned to calcium sulfate hemihydrate [26]. After further hydration treatment, the typical O–H band of calcium sulfate hemihydrate at 3612 cm^{-1} disappeared and the typical O–H bands of calcium sulfate dihydrate at 3405 and 1688 cm^{-1} appeared (c in Figure 6), indicating the transformation from calcium sulfate hemihydrate to calcium sulfate dihydrate [29]. From the results of the XRD in a in Figure 7, hydroxyapatite

(2θ = 25.9°, 28.9°, 31.7°, 34.1°, 39.8°, 46.7°, 49.5°, 53.2°) was the main component of the artificial weathering bone, which is consistent with that of archeological bones. After impregnation treatment, both calcium sulfate hemihydrate (2θ = 14.82°, 25.74°, 29.81°, and 31.86°) and hydroxyapatite were detected in b in Figure 7. The hydroxyapatite came from the bone sample itself. Calcium sulfate hemihydrate obviously comes from the suspension liquid of CSH, which is introduced during the impregnation treatment. After further hydration treatment, the diffraction peaks of calcium sulfate hemihydrate (2θ = 14.82°, 25.74°, 29.81° and 31.86°) disappeared and those for calcium sulfate dihydrate (2θ = 11.78°, 20.86°, 23.54°, and 29.26°) [30] appeared, as shown in c in Figure 7. Therefore, the specific appearance in Figure 5c is in fact the morphology of calcium sulfate dihydrate, which is the reaction product between calcium sulfate hemihydrate and water during the hydration procedure. Overall, the FTIR and the XRD results were in agreement with each other. Meanwhile, they also showed high consistency with the morphology changes displayed in Figure 5.

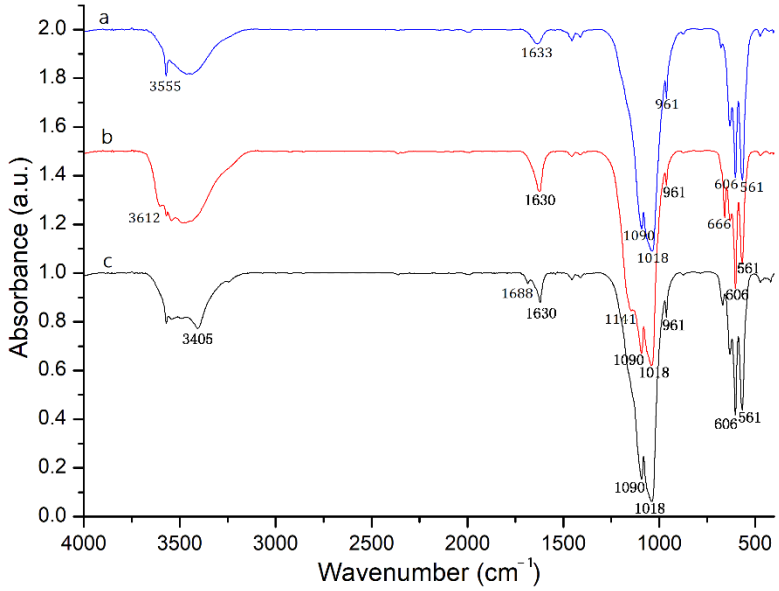

Figure 6. The FTIR results of the bone samples before and after the consolidation treatment. a. Untreated, b. treated by CSH suspension, c. treated by both the CSH suspension and water.

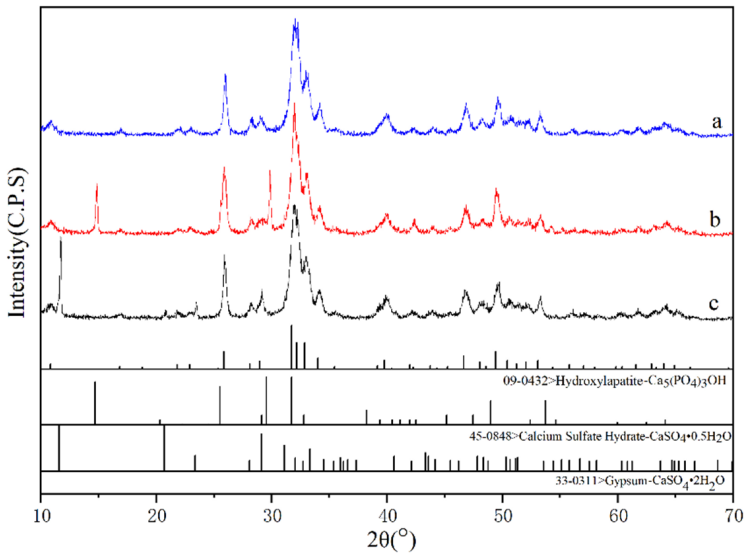

Figure 7. The XRD results of the bone samples before and after the consolidation treatment. a. Untreated, b. treated by CSH suspension, c. treated by both the CSH suspension and water.

The sectional structures of the bone samples were also observed by SEM and the results are shown in Figure 8. Before the consolidation treatment, the bone sample was rough and loose in appearance (Figure 8a). After the consolidation treatment, the bone sample became even and compact (Figure 8b). This means that the pores and cracks in the bone substrate had been filled by the calcium sulfate consolidant, which was proven further by the elemental distribution results of EDX. Sulfur was found throughout the cross section of the bone sample in Figure 8b (inset), showing a sufficient permeability of the CSH suspension. Similarly, the suspension of nano calcium hydroxide in the alcohol solvent also presented very good properties and was used in the conservation of the bone relics [10]. The small size of the nano inorganic consolidants plays an important role in these cases.

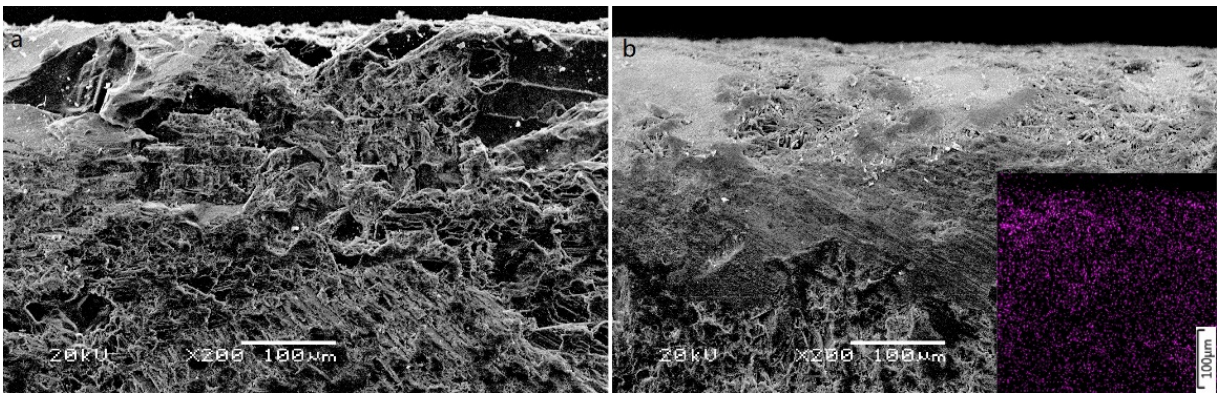

Figure 8. The cross–section of the bone samples. (**a**) Untreated, (**b**) consolidated by CSD.

The porosity, density, strength, and appearance changes were also investigated to assess the consolidation effect. After treatment, the porosity of the bone samples was reduced (Figure 9), while its density increased (Figure 10), confirming that the open pores and cracks of the bone samples were filled and the bone samples became denser. Generally, reduced porosity and increased density as a result of the reinforcement has been proven by many studies [31–33]. Surface hardness is adopted in the strength evaluation because of the inhomogeneity of the bone samples [34]. This index often refers to the deformation or damage resistance of the surface of an object. According to Figure 11, the hardness of the samples significantly increased after the consolidation treatment. This is obviously a result of the formation of CSD. After the hydration treatment, the particles of CSH were dissolved and furthered integrated together to form a continuous phase of the CSD phase [35]. Meanwhile, a strong connection was also established between the bone matrix and the produced CSD phase. Thus, the newly generated CSD phase can work as both a filling and reinforcing agent of weak bones. The change in appearance is one of the necessary evaluation indices for protective coating materials or methods used on cultural heritage [36]. It is commonly conducted by the determination of color difference. Generally, the threshold of color difference is 5.0 in the conservation of cultural heritage [37]. The color difference of the bone samples in the present study varied between 2.9 and 3.2 (Figure 12), which are all below 5.0, so are acceptable [38].

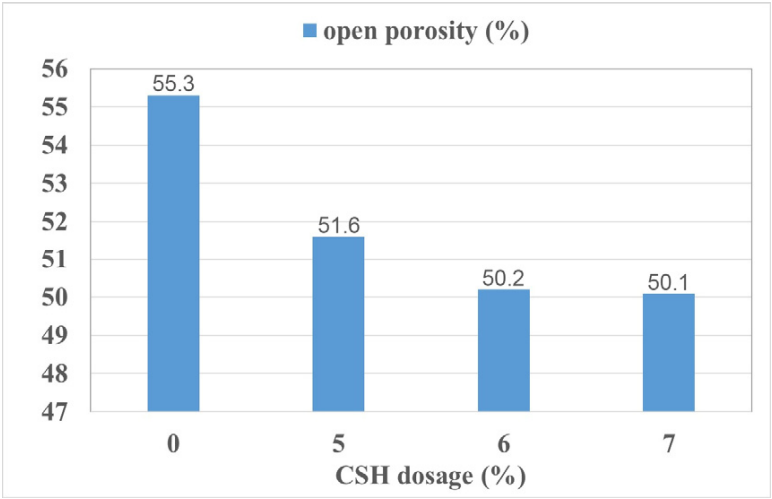

Figure 9. The open porosity change in bone with consolidation by CSH.

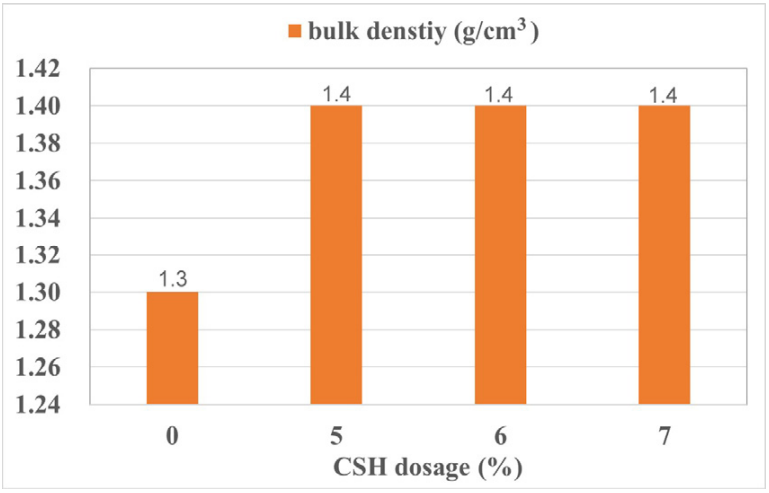

Figure 10. The bulk density change in the bone, samples after consolidation by CSH.

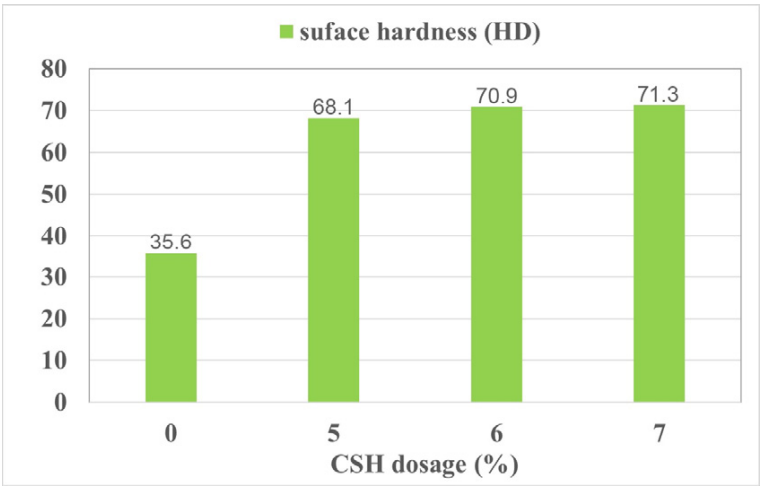

Figure 11. The surface hardness change in the bone samples after consolidation by CSH.

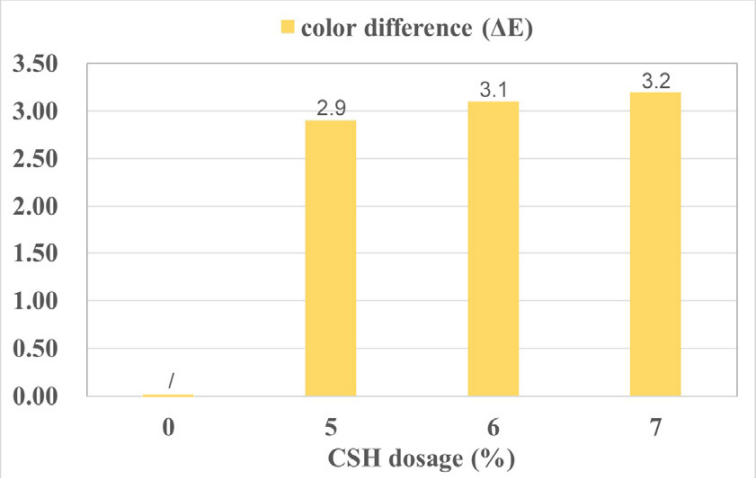

Figure 12. The color difference change in the bone samples after consolidation by CSH.

4. Conclusions

In this paper, nano CSH was successfully prepared by the reaction of calcium chloride and sulfuric acid in ethylene glycol solution. It was then re-dispersed in an alcohol solvent to obtain a suspension liquid with high kinetic stability and explored as a protective material for bone relics. In application, the suspension of CSH was first introduced into the bone samples, followed by the introduction of water, which hydrated the CSH into a continuous phase of CSD, filling the open pores, bridging the cracks, and providing additional strength for the weak bones. After the consolidation treatment, the porosity of the bone samples reduced, the strength of the bone samples increased, and the appearance change of the samples was acceptable. However, due to the low durability of gypsum in the open air, the proposed protective material is appropriate only for indoor porous weak bone objects and cannot be applied to any unsheltered or semi-sheltered objects.

Author Contributions: Conceptualization, F.Y.; Data curation, Y.L., R.L., L.H., X.W., L.W. and X.L.; Investigation, Y.L., R.L., L.H., L.W., X.L. and K.Z.; Methodology, F.Y.; Writing—original draft, Y.L.; Writing—review & editing, K.Z., R.L. and X.W. All authors have read and agreed to the published version of the manuscript.

Funding: This work was supported by the National Natural Science Foundation of China (B0501 21975202) and Key R & D Program in Shaanxi Province (2020SF-363).

Institutional Review Board Statement: Not applicable.

Informed Consent Statement: Not applicable.

Data Availability Statement: Data is contained within the article.

Conflicts of Interest: The authors declare no conflict of interest.

References

1. Liu, J.-H.; Ke, W.; Hwang, M.-C.; Chen, K.Y. Micro-Raman spectroscopy of Shang oracle bone inscriptions. *J. Archaeol. Sci. Rep.* **2021**, *37*, 102910. [CrossRef]
2. Demattè, P. The Origins of Chinese Writing: The Neolithic Evidence. *Camb. Archaeol. J.* **2010**, *20*, 211–228. [CrossRef]
3. Brunson, K.; Zhao, X.; He, N.; Dai, X.; Rodrigues, A.; Yang, D. New insights into the origins of oracle bone divination: Ancient DNA from Late Neolithic Chinese bovines. *J. Archaeol. Sci.* **2016**, *74*, 35–44. [CrossRef]
4. Anzhu, L. Oracle-Bone Inscriptions and Cultural Memory. *Front. Art Res.* **2020**, *2*, 63–73. [CrossRef]
5. Wang, K.; Hu, D.B. Hydroxyapatite: Collagen Biomimetic Composite Material in Conservation of Tortoise Shell Relics. *J. Natl. Mus. China* **2013**, *3*, 141–152.
6. Pérez, L.; Sanchis, A.; Hernández, C.M.; Galván, B.; Sala, R.; Mallol, C. Hearths and bones: An experimental study to explore temporality in archaeological contexts based on taphonomical changes in burnt bones. *J. Archaeol. Sci. Rep.* **2017**, *11*, 287–309. [CrossRef]

7. Kibblewhite, M.; Tóth, G.; Hermann, T. Predicting the preservation of cultural artefacts and buried materials in soil. *Sci. Total Environ.* **2015**, *529*, 249–263. [CrossRef]
8. López-Polín, L. Possible interferences of some conservation treatments with subsequent studies on fossil bones: A conservator's overview. *Quat. Int.* **2011**, *275*, 120–127. [CrossRef]
9. Han, X.; Huang, X.; Zhang, B. Morphological studies of menthol as a temporary consolidant for urgent conservation in archaeological field. *J. Cult. Herit.* **2016**, *18*, 271–278. [CrossRef]
10. Natali, I.; Tempesti, P.; Carretti, E.; Potenza, M.; Sansoni, S.; Baglioni, P.; Dei, L. Aragonite Crystals Grown on Bones by Reaction of CO_2 with Nanostructured $Ca(OH)_2$ in the Presence of Collagen. Implications in Archaeology and Paleontology. *Langmuir* **2014**, *30*, 660–668. [CrossRef]
11. North, A.; Balonis, M.; Kakoulli, I. Biomimetic hydroxyapatite as a new consolidating agent for archaeological bone. *Stud. Conserv.* **2016**, *61*, 146–161. [CrossRef]
12. Gong, W.; Yang, S.; Zheng, L.; Xiao, H.; Zheng, J.; Wu, B.; Zhou, Z. Consolidating effect of hydroxyapatite on the ancient ivories from Jinsha ruins site: Surface morphology and mechanical properties study. *J. Cult. Heritage* **2019**, *35*, 116–122. [CrossRef]
13. Liu, Y.; Hu, Q.; Zhang, K.; Yang, F.; Yang, L.; Wang, L. In-situ growth of calcium sulfate dihydrate as a consolidating material for the archaeological bones. *Mater. Lett.* **2021**, *282*, 128713. [CrossRef]
14. Milivojević, M. Excavation, reconstruction and conservation of steppe elephant from the clay pit of the building material factory "Toza Marković" at Kikinda (Serbia). *Bull. Nat. Hist. Mus.* **2011**, *4*, 51–64.
15. Ahmed, H.T. Restoration of historical artifacts and made available for exhibition in museums. *J. Am. Sci.* **2015**, *12*, 183–192.
16. Qin, Z.F. Restoration of a bronze grain receptacle with the pattern of Panhui (Spring and Autumn period). *J. Chinaese Antiq.* **2020**, *5*, 74–76.
17. Liu, Y.; Yang, F.; Wang, L. Exploratory research about the selective cleaning of calcium sulfate sediments on archaeological potteries. *New J. Chem.* **2020**, *44*, 7412–7416. [CrossRef]
18. Park, Y.B.; Mohan, K.; Al-Sanousi, A.; Almaghrabi, B.; Genco, R.J.; Swihart, M.T.; Dziak, R. Synthesis and characterization of nanocrystalline calcium sulfate for use in osseous regeneration. *Biomed. Mater.* **2011**, *6*, 055007. [CrossRef]
19. Hazra, C.; Bari, S.; Kundu, D.; Chaudhari, A.; Mishra, S.; Chatterjee, A. Ultrasound-assisted/biosurfactant-templated size-tunable synthesis of nano-calcium sulfate with controllable crystal morphology. *Ultrason. Sonochem.* **2014**, *21*, 1117–1131. [CrossRef]
20. Yin, S.; Yang, L. α or β?-hemihydrates transformed from dihydrate calcium sulfate in a salt-mediated glycerol–water solution. *J. Cryst. Growth* **2020**, *550*, 125885. [CrossRef]
21. Fu, H.; Jiang, G.; Wang, H.; Wu, Z.; Guan, B. Solution-Mediated Transformation Kinetics of Calcium Sulfate Dihydrate to α-Calcium Sulfate Hemihydrate in $CaCl_2$ Solutions at Elevated Temperature. *Ind. Eng. Chem. Res.* **2013**, *52*, 17134–17139. [CrossRef]
22. Leukel, S.; Panthöfer, M.; Mondeshki, M.; Schärtl, W.; Ruiz, S.P.; Tremel, W.; Schaertl, W. Calcium Sulfate Nanoparticles with Unusual Dispersibility in Organic Solvents for Transparent Film Processing. *Langmuir* **2018**, *34*, 7096–7105. [CrossRef] [PubMed]
23. Borsoi, G.; Lubelli, B.; van Hees, R.; Veiga, R.; Silva, A.S.; Colla, L.; Fedele, L.; Tomasin, P. Effect of solvent on nanolime transport within limestone: How to improve in-depth deposition. *Colloids Surf. A Physicochem. Eng. Asp.* **2016**, *497*, 171–181. [CrossRef]
24. Yang, F.; Zhang, B.; Liu, Y.; Wei, G.; Zhang, H.; Chen, W.; Xu, Z. Biomimic conservation of weathered calcareous stones by apatite. *New J. Chem.* **2011**, *35*, 887–892. [CrossRef]
25. Figueiredo, M.; Fernando, A.; Martins, G.; Freitas, J.; Judas, F. Effect of the calcination temperature on the composition and microstructure of hydroxyapatite derived from human and animal bone. *Ceram. Int.* **2010**, *36*, 2383–2393. [CrossRef]
26. Chen, X.; Wu, Q.; Gao, J.; Tang, Y. Hydration characteristics and mechanism analysis of β-calcium sulfate hemihydrate. *Constr. Build. Mater.* **2021**, *296*, 123714. [CrossRef]
27. Saha, A.; Lee, J.; Pancera, S.M.; Bräeu, M.F.; Kempter, A.; Tripathi, A.; Bose, A. New Insights into the Transformation of Calcium Sulfate Hemihydrate to Gypsum Using Time-Resolved Cryogenic Transmission Electron Microscopy. *Langmuir* **2012**, *28*, 11182–11187. [CrossRef]
28. Youness, R.A.; Taha, M.A.; Elhaes, H.; Ibrahim, M. Molecular modeling, FTIR spectral characterization and mechanical properties of carbonated-hydroxyapatite prepared by mechanochemical synthesis. *Mater. Chem. Phys.* **2017**, *190*, 209–218. [CrossRef]
29. Ding, X.; Wei, B.; Deng, M.; Chen, H.; Shan, Z. Effect of protein peptides with different molecular weights on the setting and hydration process of gypsum. *Constr. Build. Mater.* **2022**, *318*, 126185. [CrossRef]
30. Pan, Z.; Lou, Y.; Yang, G.; Ni, X.; Chen, M.; Xu, H.; Miao, X.; Liu, J.; Hu, C.; Huang, Q. Preparation of calcium sulfate dihydrate and calcium sulfate hemihydrate with controllable crystal morphology by using ethanol additive. *Ceram. Int.* **2013**, *39*, 5495–5502. [CrossRef]
31. Ibrahim, M.M.; Mohamed, W.S.; Mohamed, H.M. Evaluation of the efficacy of traditional and nano paraloid b72 for pottery consolidation. *Int. J. Conserv. Sci.* **2022**, *13*, 15–30.
32. Al-Dosari, M.A.; Darwish, S.; El-Hafez, M.A.; Elmarzugi, N.; Al-Mouallimi, N.; Mansour, S. Effects of Adding Nanosilica on Performance of Ethylsilicat (TEOS) as Consolidation and Protection Materials for Highly Porous Artistic Stone. *J. Mater. Sci. Eng. A* **2016**, *6*, 192–204. [CrossRef]
33. Terzu, R.; Baraj, E.; Förester, C.; Kropf, H.; Xhaxhiu, K.; Come, M. Ananalytical study of marble consolidation by oxalate precipitation using density, ftir and powder-xrd measurements. *J. Eng. Process. Manag.* **2017**, *8*, 21–26. [CrossRef]

34. Luo, C.; Liao, J.; Zhu, Z.; Wang, X.; Lin, X.; Huang, W. Analysis of Mechanical Properties and Mechanical Anisotropy in Canine Bone Tissues of Various Ages. *BioMed Res. Int.* **2019**, *2019*, 3503152. [CrossRef] [PubMed]
35. Van Driessche, A.E.S.; Benning, L.G.; Rodriguez-Blanco, J.D.; Ossorio, M.; Bots, P.; García-Ruiz, J.M. The Role and Implications of Bassanite as a Stable Precursor Phase to Gypsum Precipitation. *Science* **2012**, *336*, 69–72. [CrossRef] [PubMed]
36. Martínez, M.; Calero, A.I.; Valero, E.M. Colorimetric and spectral data analysis of consolidants used for preservation of medieval plasterwork. *J. Cult. Heritage* **2020**, *42*, 64–71. [CrossRef]
37. Ferreira Pinto, A.P.; Rodrigues, J.D. Impacts of consolidation procedures on colour and absorption kinetics of carbonate stones. *Stud. Conserv.* **2014**, *59*, 79–90. [CrossRef]
38. Concha-Lozano, N.; Lafon, D.; Sabiri, N.; Gaudon, P. Color thresholds for aesthetically compatible replacement of stones on monuments. *Color Res. Appl.* **2013**, *38*, 356–363. [CrossRef]